

Article

Tidal Datum Changes Induced by Morphological Changes of North Carolina Coastal Inlets

Jindong Wang ^{1,2,*} and Edward Myers ¹

¹ Coast Survey Development Laboratory, National Ocean Service, National Oceanic and Atmospheric Administration, 1315 East-West Highway, Silver Spring, MD 20910, USA; edward.myers@noaa.gov

² Earth Resources Technology, Inc., 14401 Sweitzer Lane, Suite 300, Laurel, MD 20707, USA

* Correspondence: jindong.wang@gmail.com; Tel.: +1-301-713-2809

Academic Editor: Richard P. Signell

Received: 18 July 2016; Accepted: 12 November 2016; Published: 18 November 2016

Abstract: In support of the National Oceanic and Atmospheric Administration's VDatum program, a new version of a tidal datum product for the North Carolina coastal waters has been developed to replace the initial version released in 2004. Compared with the initial version, the new version used a higher resolution grid to cover more areas and incorporated up-to-date tide, bathymetry, and shoreline data. Particularly, the old bathymetry datasets that were collected from the 1930s to the 1970s and were used in the initial version have been replaced by the new bathymetry datasets collected in the 2010s in the new version around five North Carolina inlets. This study aims at evaluating and quantifying tidal datum changes induced by morphological changes over about 40 to 80 years around the inlets. A series of tidal simulations with either the old or new bathymetry datasets used around five inlets were conducted to quantify the consequent tidal datum changes. The results showed that around certain inlets, approximately 10% change in the averaged depth could result in over 30% change in the tidal datum magnitude. Further investigation also revealed that tidal datum changes behind the barrier islands are closely associated with the cross-inlet tidal flux changes.

Keywords: VDatum; tidal datums; morphological changes; inlets; North Carolina

1. Introduction

The software package VDatum, developed and maintained by the National Oceanic and Atmospheric Administration (NOAA), allows users to transform geospatial data among a variety of ellipsoidal, orthometric, and tidal datums [1]. For example, users can integrate the United States Geological Survey's elevation data referenced to the North American Vertical Datum of 1988 (NAVD88) with NOAA's sounding data referenced to Mean Lower Low Water (MLLW) to build a seamless bathymetry-topography Digital Elevation Model (DEM) dataset referenced to a common datum of Mean Sea Level (MSL) by using VDatum. The integrated DEM provides a basis for coastal inundation modeling and mapping [2].

As a critical part of VDatum, tidal datums are derived from water level time series simulated by a tide model. The tidal highs and lows from modeled water levels are used to calculate tidal datums: Mean Higher High Water (MHHW), Mean High Water (MHW), Mean Low Water (MLW), and Mean Lower Low Water (MLLW) [3]. Following the VDatum Standard Operating Procedures [4], we use the ADvanced CIRCulation (ADCIRC) model [5] to conduct tidal simulations for deriving tidal datums in VDatum. The ADCIRC model has been widely used for tidal simulations from the basin scale [6–8] to the regional scale [9–11].

The initial version of VDatum for North Carolina was released in 2004 [12]. An updated version has been developed to cover more areas and incorporate up-to-date tide, bathymetry, and shoreline

data. Around five main North Carolina inlets (Beaufort, Barden, Ocracoke, Hatteras, and Oregon Inlet), the bathymetry datasets collected from the 1930s to the 1970s were used in the initial version for tide modeling to derive tidal datums. These old bathymetry datasets have been replaced by the datasets collected in the 2010s around five inlets in the updated version. Tidal datum changes induced by morphological changes of the inlets need to be quantified to provide NOAA guidance for future updating of VDatum, installing new tide gauges, and conducting new hydrographic surveys in this region.

Tidal inlets are typically dynamically active regions where tidal circulation and transport lead to continuous sediment movement and thus morphological changes. In general, the combination of tides and waves was considered to shape the inlet morphology into different types: flood-tidal delta and ebb-tidal delta [13–16]. Tidal distortion was found to affect net sediment transport [17,18]. Tidal prism and inlet cross-sectional area were also considered as important factors to affect the inlet morphology [19]. Around North Carolina's Beaufort Inlet, a nearshore jet in tidal circulation was identified and simulated and was considered to be associated with the net transport through the inlet [20,21]. Sediment deposition and erosion around North Carolina inlets was investigated with the local dynamics by Inman and Dolan [22]. These previous studies have mainly been focused on how hydrodynamics (e.g., tides and waves) affect the morphology of the inlets. Little attention has been paid to the feedback of tides to morphological changes of the inlets.

In this study, we aimed at evaluating and quantifying how morphological changes of the inlets affect tidal changes. This paper is organized as follows: following the introduction section, Section 2 describes the sources of a variety of tide, shoreline, and bathymetry data, as well as the tide model setup, numerical experiment design, and model validation. The results will be described in Section 3 followed by some discussions and conclusions in the last section.

2. Materials and Methods

2.1. Data Sources

The water level data [23] and the observed tidal datums [24] provided by the Center for Operational Oceanographic Products and Services (CO-OPS) of NOAA were used for model validation. CO-OPS typically publishes one single value for a particular tidal datum (e.g., MHW) at one station. The tidal datums were typically derived from the water level time series for a certain time period (from a couple of months to years). The observed tidal datums were referenced to the current National Tidal Datum Epoch (NTDE) (1983–2001) [24]. In this paper, the observed tidal datums at 31 tide stations were compared with the modeled tidal datums to evaluate the general model performance in North Carolina coastal waters. Since the identification (ID) numbers of all North Carolina stations begin with 865, the 865 will be ignored when we describe station IDs in the following discussions.

The locations of all 31 datum stations are shown in Figure 1. Among these stations, the 4 outside stations 1370, 4400, 6590, and 6937 are located on the Atlantic Ocean coast. The other 27 inside stations are located behind the barrier islands and within the sounds and estuaries. Among the 31 datum stations, tidal harmonic constituents are also provided for 16 stations [25]. In addition, the hourly water level data collected from 1967 to 2016 at Beaufort Station (ID: 6483), about 4 km behind the Beaufort Inlet and Duck Station (ID: 1370) on the Atlantic coast, were used to evaluate the temporal variation of MHW.

The development of the hydrodynamic model grid requires shoreline and bathymetry data. The National Geodetic Survey provided the up-to-date North Carolina shoreline data which combined NOAA Continually Updated Shoreline Product (CUSP) and the Office of Coast Survey (OCS) chart shoreline data [26]. The bathymetry data were mainly from three sources. The OCS sounding data collected from 1851 to 2012 were used for most of the North Carolina coastal regions. The particular areas covered by the datasets collected in a certain year can be found in a Bathymetry Data Viewer [27]. A global bathymetry-topography database SRTM30_PLUS from Scripps Institution of Oceanography

was used for the far offshore region [28]. The sounding data collected since 2010 by the U.S. Army Corps Engineers’ Wilmington District were used for coastal inlets and intra-coastal waterways [29]. All the up-to-date tide, bathymetry, and shoreline data have been applied to derive the updated tidal datums used by the currently available VDatum tool.

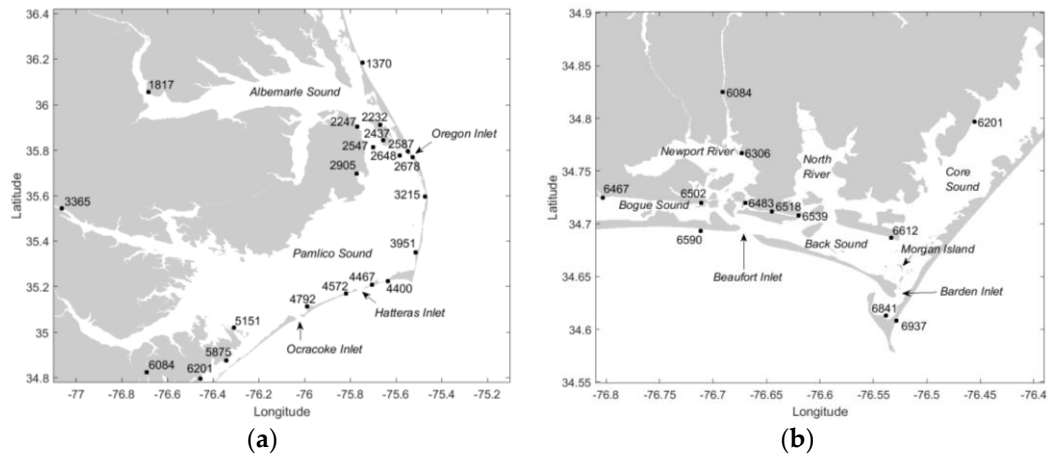


Figure 1. Map of North Carolina coastal waters and inlets and the locations of the National Oceanic and Atmospheric Administration (NOAA) water level stations (black dots): (a) Northern part; (b) Southern part. Please note that the scale in (b) is 4 times larger than (a).

2.2. Model Setup

The ADCIRC [5] Two-Dimensional Depth Integrated (2DDI) version was used in this study to solve the shallow water equations and simulate tidal water levels. The finite amplitude and convection terms and the wetting and drying option were activated. The lateral viscosity was set as a constant, $5.0 \text{ m}\cdot\text{s}^{-2}$, throughout the model domain. The quadratic bottom friction scheme was used with a constant coefficient of 0.0025. The model was forced by a reconstructed tide at the ocean boundary (shown as blue lines in Figure 2a) using the harmonic constants of the five most significant tidal constituents (M_2 , S_2 , N_2 , K_1 , and O_1) from the EC2001 tidal database [7].

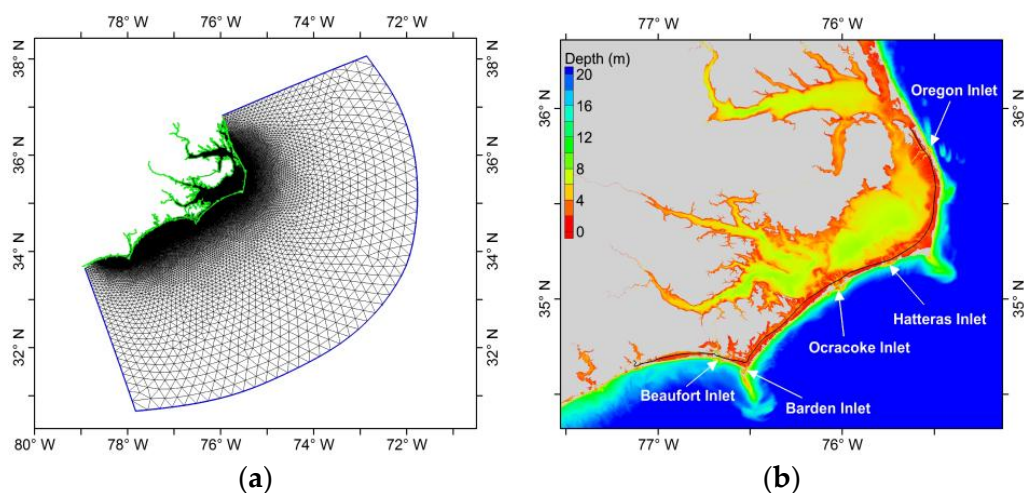


Figure 2. (a) The triangular model grid (the blue lines delineate the open ocean boundary; the green lines delineate the land boundary); (b) Model grid bathymetry in North Carolina coastal waters (the regions deeper than 20 m use the same blue color; the black line shows the location for longitudinal profiles in Figures 15 and 16).

The time step was set to be 1 s. Under this condition, the maximum Courant number is 0.67 over the smallest elements in the grid. This ensured model stability. The model simulations covered a time period of 40 days. The first 10 days were used for the tidal field to reach an equilibrium state. The 6-min water level time series at each node from the last 30 days of each simulation were then used to derive tidal datums and harmonic constants. The 15-min velocity time series at each node from the last 15 days of each simulation were used to calculate the flood and ebb fluxes across the inlets.

A triangular mesh (Figure 2a) has been developed with a spatially varying resolution from 30 km offshore to 10 m inland to resolve important geographical features such as inlets, channels, estuaries, and bays. We used this mesh as a basis to generate the model grids by interpolating the old (1930s–1970s) and the new (2010s) bathymetry datasets around five North Carolina inlets (Beaufort, Barden, Ocracoke, Hatteras, and Oregon Inlet) onto the mesh. In the following discussions, we will use the old-bathy grid to represent the model grid using the old (1930s–1970s) bathymetry data and use the new-bathy grid to represent the model grid using the new (2010s) bathymetry data around the inlets. The particular collection years for the old and new bathymetry datasets around each inlet have been listed in Table 1. For the old-bathy grid, we combined the patched bathymetry datasets collected in 1956 and 1962 around Ocracoke Inlet to represent the general morphology in this region in the mid-20th century. For the new-bathy grid, we combined the bathymetry datasets collected in 2014, 2015, and 2016 around Hatteras Inlet and the bathymetry datasets collected in 2014 and 2016 around Oregon Inlet to represent the recent morphology in these two regions. The detailed coverages of the old and the new bathymetry datasets are shown for Beaufort and Barden Inlet in Figure 3d, Ocracoke and Hatteras Inlet in Figure 4d, and Oregon Inlet in Figure 5d. Other than the inlet regions delineated by the polygons in Figures 3–5, the old-bathy grid and the new-bathy grid have the same depths interpolated from the same bathymetry datasets described in Section 2.1. Therefore, the only difference between the old-bathy grid and the new-bathy grid was the bathymetry around the five inlets.

Table 1. Bathymetric data and morphological parameters around five North Carolina inlets.

Inlet	Width (km)	Area with Changed Bathymetry (km ²)	Collection Years of Old Bathymetry	Mean Depth of Old-Bathy (m)	Collection Years of New Bathymetry	Mean Depth of New-Bathy (m)
Beaufort	1.3	6.2	1953	5.0	2010	7.2
Barden	0.7	4.3	1955	1.7	2015	2.9
Ocracoke	2.4	8.8	1956, 1962	4.0	2013	4.9
Hatteras	2.2	8.7	1935	2.6	2014, 2015, 2016	2.7
Oregon	1.0	3.7	1975	3.6	2014, 2016	4.0

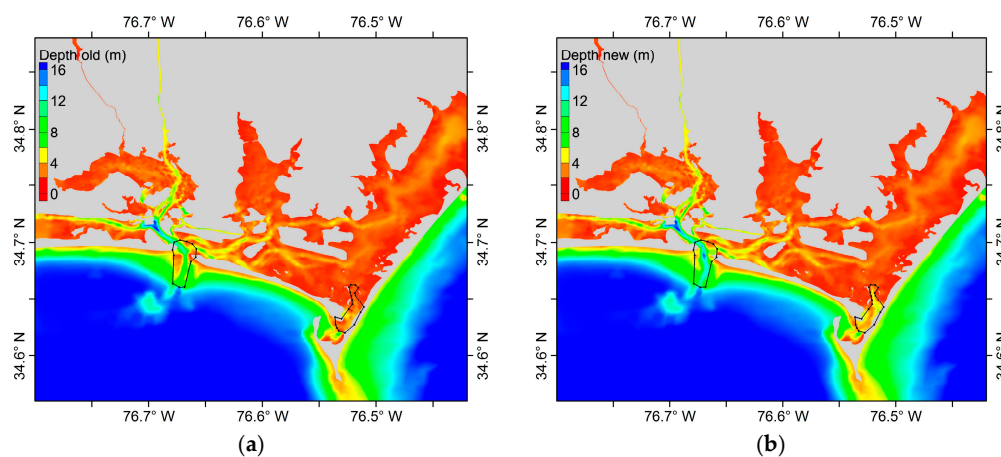


Figure 3. *Cont.*

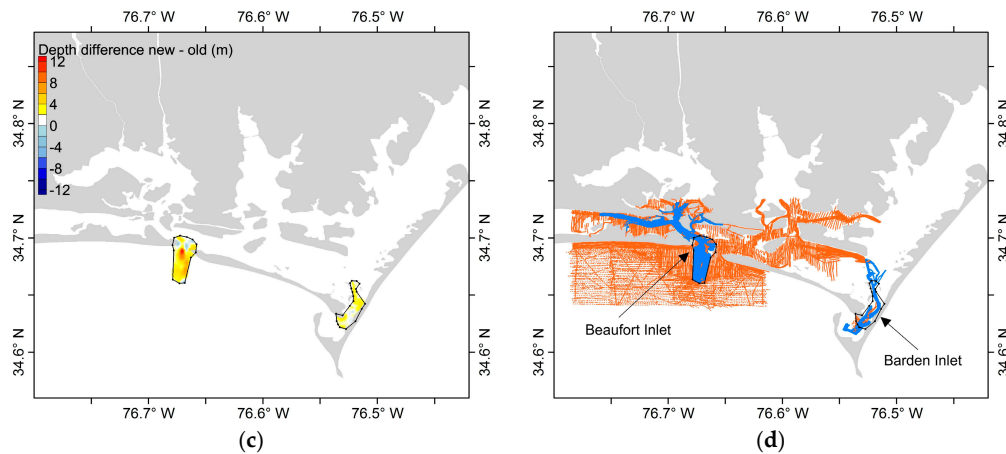


Figure 3. The morphological changes around Beaufort Inlet and Barden Inlet: (a) the old-bathy grid depths; (b) the new-bathy grid depths; (c) the depth difference between the new-bathy grid and the old-bathy grid; (d) the original bathymetry sounding data points (orange: data in 1953 around Beaufort Inlet and data in 1955 around Barden Inlet; blue: data in 2010 around Beaufort Inlet and data in 2015 around Barden Inlet). The black dotted polygons delineate the area with changed bathymetry.

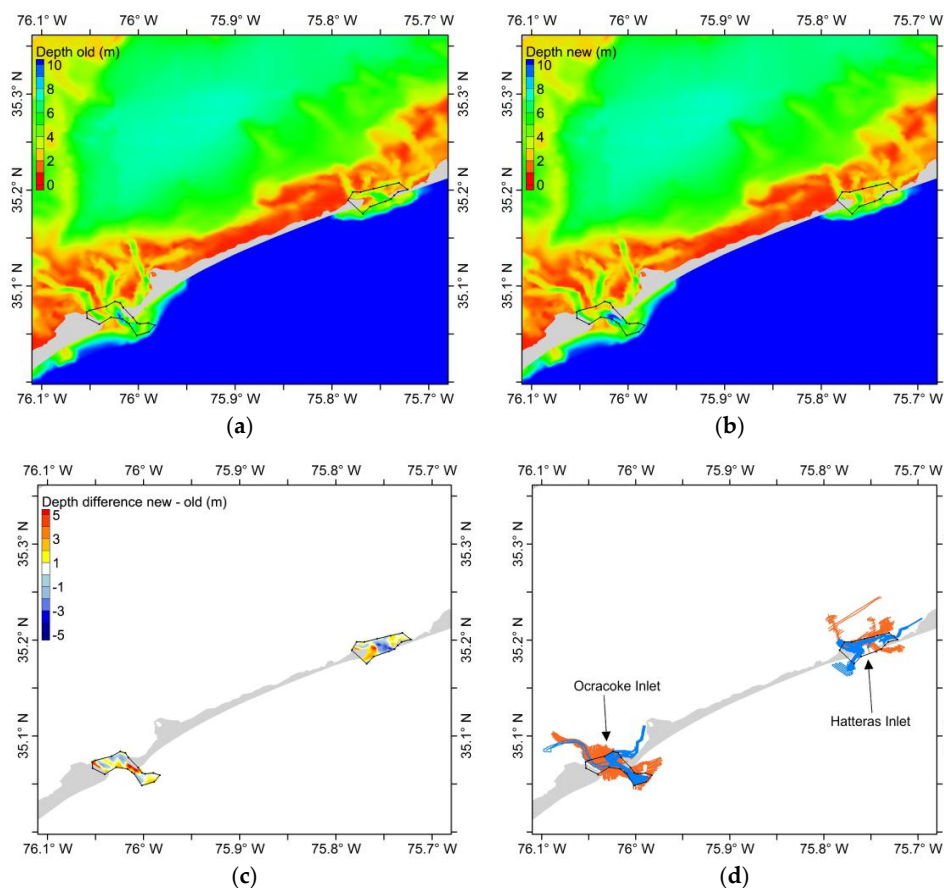


Figure 4. The morphological changes around Ocracoke Inlet and Hatteras Inlet: (a) the old-bathy grid depths; (b) the new-bathy grid depths; (c) the depth difference between the new-bathy grid and the old-bathy grid; (d) the original bathymetry sounding data points (orange: data in 1956 and 1962 around Ocracoke Inlet and data in 1935 around Hatteras Inlet; blue: data in 2013 around Ocracoke Inlet and data in 2014, 2015, and 2016 around Hatteras Inlet). The black dotted polygons delineate the area with changed bathymetry.

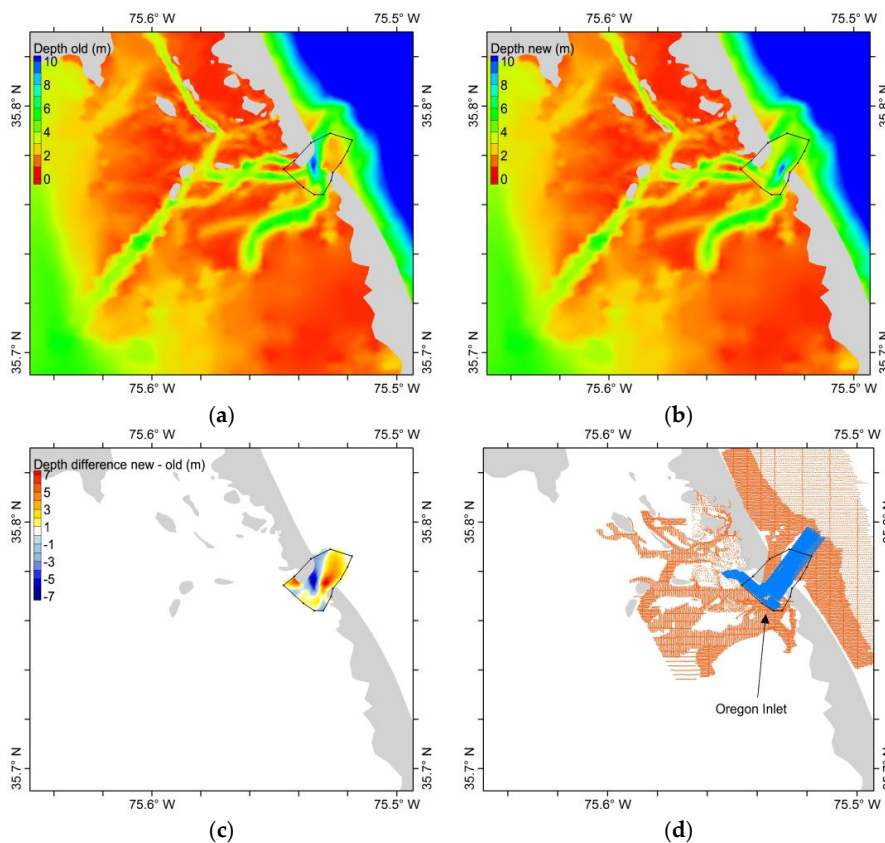


Figure 5. The morphological changes around Oregon Inlet: (a) the old-bathy grid depths; (b) the new-bathy grid depths; (c) the depth difference between the new-bathy grid and the old-bathy grid; (d) the original bathymetry sounding data points (orange: data in 1975 around Oregon Inlet; blue: data in 2014 and 2016 around Oregon Inlet). The black dotted polygons delineate the area with changed bathymetry.

The same model setup and tidal forcing were applied to the models using the old-bathy grid and the new-bathy grid. In the following discussions, we will use the old-bathy model and the new-bathy model to represent the models using the old-bathy grid and the new-bathy grid, respectively.

Since Beaufort Inlet and Barden Inlet are close to each other, we made another two grids new-bathy-BE and new-bathy-BA to evaluate the tidal datum changes induced by the morphological changes of each individual inlet. For the new-bathy-BE grid, the new bathymetry data were used around Beaufort Inlet and the old bathymetry data were used for the other four inlets. Similarly, for the new-bathy-BA grid, the new bathymetry data were used around Barden Inlet and the old bathymetry data were used for the other four inlets. We will use the new-bathy-BE model and the new-bathy-BA model to represent tidal simulations using the new-bathy-BE grid and the new-bathy-BA grid, respectively, in the following discussions.

The overview of the common area bathymetry is shown in Figure 2b. Most regions behind the barrier islands are shallower than 8 m. There are significant bathymetric differences between the old-bathy grid and the new-bathy grid around the inlets, as shown in Figures 3–5. For example, around Beaufort Inlet (Figure 3), the mean depth has increased by 44% from the old-bathy depth of 5.0 m to the new-bathy depth of 7.2 m. In addition, the recent deep channel became deeper and wider relative to about 60 years ago. These morphological changes around Beaufort Inlet should be mainly associated with historical dredging activities [30]. The mean depths increased by 70%, 22%, 4%, and 11% from the old-bathy grid to the new-bathy grid around Barden Inlet, Ocracoke Inlet, Hatteras Inlet, and Oregon Inlet, respectively. The morphological parameters for five inlets are listed in Table 1.

2.3. Model Validation

Computed tidal datums from both the old-bathy model and the new-bathy model were compared with the observed tidal datums at 31 stations. The root mean squared errors (RMSEs) of both models for four tidal datums have been listed in Table 2. In general, both models had decent performances relative to the observations. The new-bathy model had a little higher overall performance than the old-bathy model. It should be noted that the RMSEs of the new-bathy model are slightly higher than the uncertainty values published on the VDatum website [31]. This is mainly because the official VDatum tidal datums were calculated from longer time series of simulated water levels.

Table 2. The root mean squared errors of the modeled tidal datums relative to the observed ones.

Model	Mean Higher High Water (MHHW) (cm)	Mean High Water (MHW) (cm)	Mean Low Water (MLW) (cm)	Mean Lower Low Water (MLLW) (cm)
Old-bathy Model	6.1	4.6	4.5	6.0
New-bathy Model	4.8	3.5	3.3	4.5

Since the four tidal datums have similar trend and patterns, only MHW will be discussed as an example in the rest of the paper. The result for MHW is shown in Figure 6. The new-bathy model outperformed the old-bathy model at particular stations. At the inside stations not too far away from the inlets (e.g., 2678, 6084, and 6483), the new-bathy model matched the observations very well while the old-bathy model underestimated the observations by approximately 5% to 25%. This is because tidal datums at these stations had changed more dramatically than other stations and the new-bathy model simulation is closer to the current National Tidal Datum Epoch (1983–2001) conditions. At the outside stations and the inside stations far away from the inlets (e.g., 1370, 3365, and 6590), the MHW values from both models had very small differences.

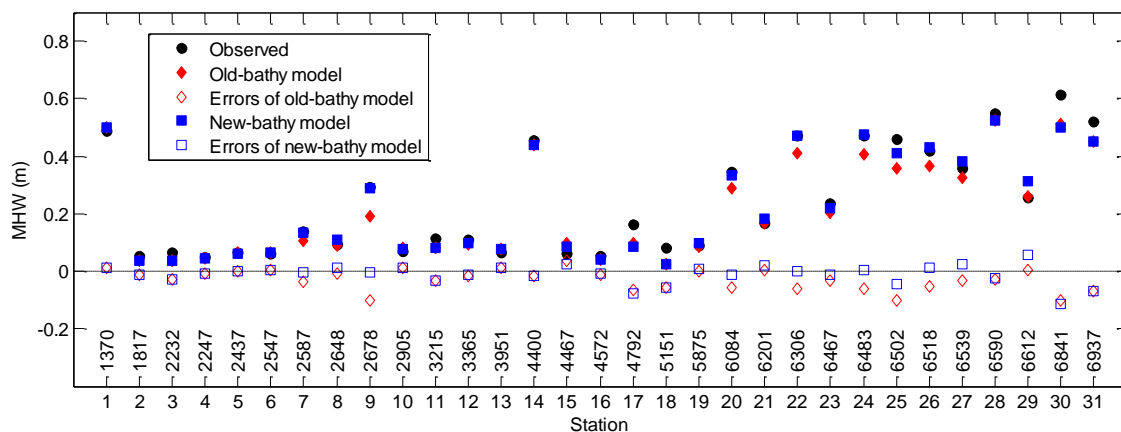


Figure 6. Comparison of MHW at 31 NOAA stations between the observations (black dots), the old-bathy model (red solid diamonds), and the new-bathy model (blue solid squares). The blank diamonds and squares indicate the model errors.

The amplitudes and phases of five principal tidal constituents (M_2 , S_2 , N_2 , K_1 , and O_1) from both models were also compared with the observations at 16 stations. As an example, the results for M_2 (Figures 7 and 8) indicate that the old-bathy model and the new-bathy model had decent performance. For some stations with small amplitude (e.g., 5875), the discrepancy between the modeled phase and the observed phase could be relatively high because the obscured tidal signals in the observed water level time series led to high uncertainty in the observed phase itself.

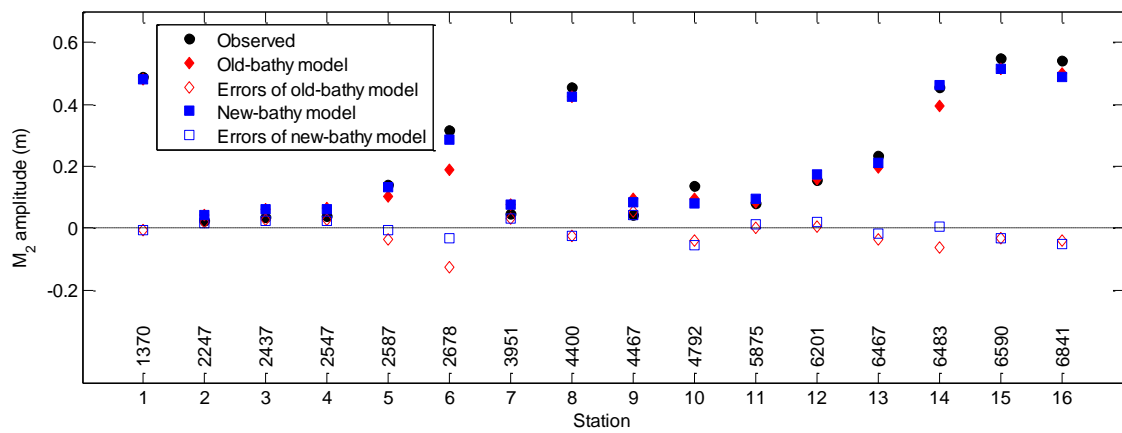


Figure 7. Comparison of the M₂ amplitude at 16 NOAA stations between the observations (black dots), the old-bathy model (red solid diamonds), and the new-bathy model (blue solid squares). The blank diamonds and squares indicate the model errors.

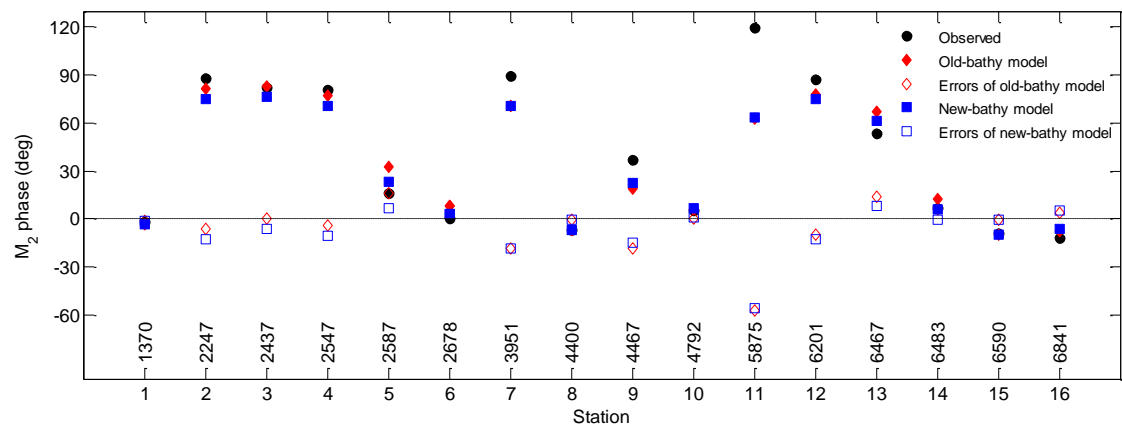


Figure 8. Comparison of the M₂ phase at 16 NOAA stations between the observations (black dots), the old-bathy model (red solid diamonds), and the new-bathy model (blue solid squares). The blank diamonds and squares indicate the model errors.

At the inside stations not too far away from the inlets (e.g., 2678 and 6483), the new-bathy model outperformed the old-bathy model. The old-bathy model had underestimated amplitudes and overestimated phases relative to the observations.

Tidal datum changes induced by morphological changes of Beaufort Inlet can also be observed from Beaufort Station (6483) about 4 km behind the Beaufort Inlet as shown in Figure 9a. The value of each black dot in the figure came from the monthly averaged MHW. In addition to the 18.6-year-cycle and seasonal variations, there was an obvious trend increasing from ~0.44 m in 1967 to ~0.49 m in 2016. The 18.6-year-cycle variation is due to the changing locations of the sun and the moon relative to the earth [2]. For the model results around the same location, MHW increased from 0.41 m of the old-bathy model to 0.47 m of the new-bathy model, which is largely consistent with the observed trend. As a comparison, for Duck Station (1370) on the Atlantic coast, MHW also showed the 18.6-year-cycle and seasonal variations and a slightly decreasing trend based on the analyzed data in 1978–2016 (Figure 9b). This trend is not reflected in the model results because Duck Station is approximately 50 km away from the nearest Oregon Inlet and thus is not affected by the inlet bathymetry changes.

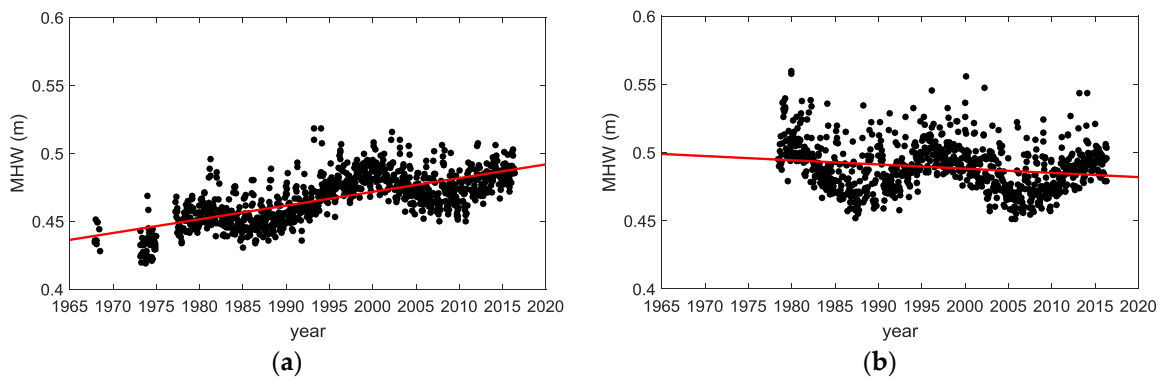


Figure 9. Temporal changes for the last few decades of the monthly averaged MHW at two NOAA stations: (a) Beaufort Station (ID: 6483); (b) Duck Station (ID: 1370). The red lines delineate the linearly best fit lines.

3. Results

3.1. Tidal Datum Changes Due to Morphological Changes of the Inlets

The MHW from the new-bathy model and the old-bathy model and their differences for the North Carolina coastal waters are shown in Figures 10–14. In general, MHW had higher values on the Atlantic Ocean side and lower values behind barrier islands. The MHW values were also higher behind Beaufort Inlet than those behind the other four inlets, indicating that it is much easier for the tides to propagate from the ocean into the sounds through Beaufort Inlet. In addition, the waters behind Beaufort Inlet have smaller areas and deeper depths relative to Pamlico Sound behind Ocracoke Inlet, Hatteras Inlet, and Oregon Inlet. Thus, tidal energy there is much less dissipated than that within Pamlico Sound.

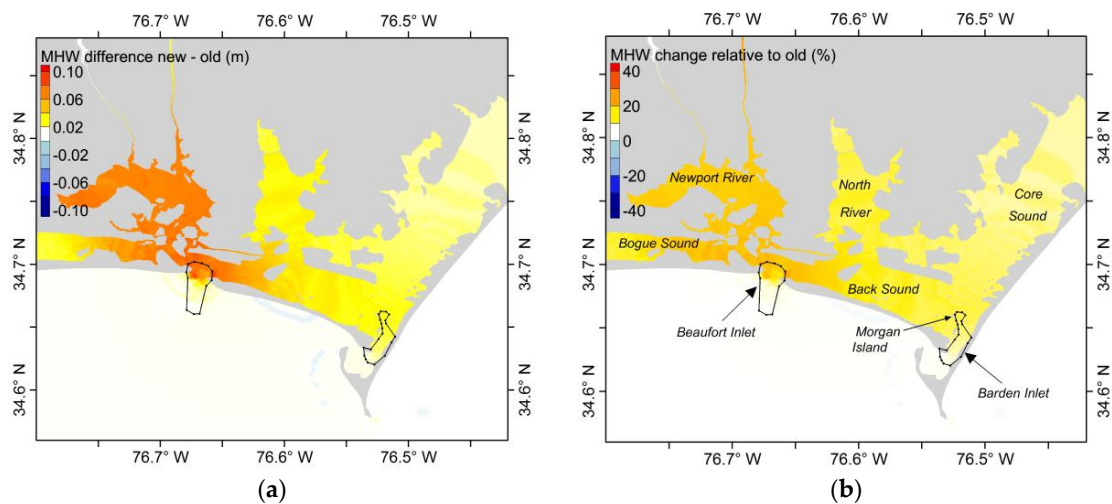


Figure 10. The MHW changes induced only by the inlet morphological changes around Beaufort Inlet: (a) the MHW difference between the new-bathy-BE model and the old-bathy model; (b) the MHW change in percentage relative to the old-bathy model MHW. The black dotted polygons delineate the area with changed bathymetry.

As shown in Figure 10, if the morphological changes only occurred around Beaufort Inlet (i.e., the new-bathy-BE model), MHW has increased behind Beaufort Inlet in three directions: Newport River, Bogue Sound, and Back Sound. MHW in the entire Newport River has increased by ~15% from ~0.4 m to ~0.46 m. The increased MHW becomes smaller where it is farther away from the inlet entrance in

both the Bogue Sound and Back Sound directions. The percentage of the increased MHW relative to the old MHW drops to 10% about 10 km away from the inlet entrance in the Bogue Sound direction and about 5 km in the Back Sound direction. Thus, the inlet morphological changes have more influence on MHW in the Newport River direction than the other two directions. This is probably because Newport River is a more enclosed area.

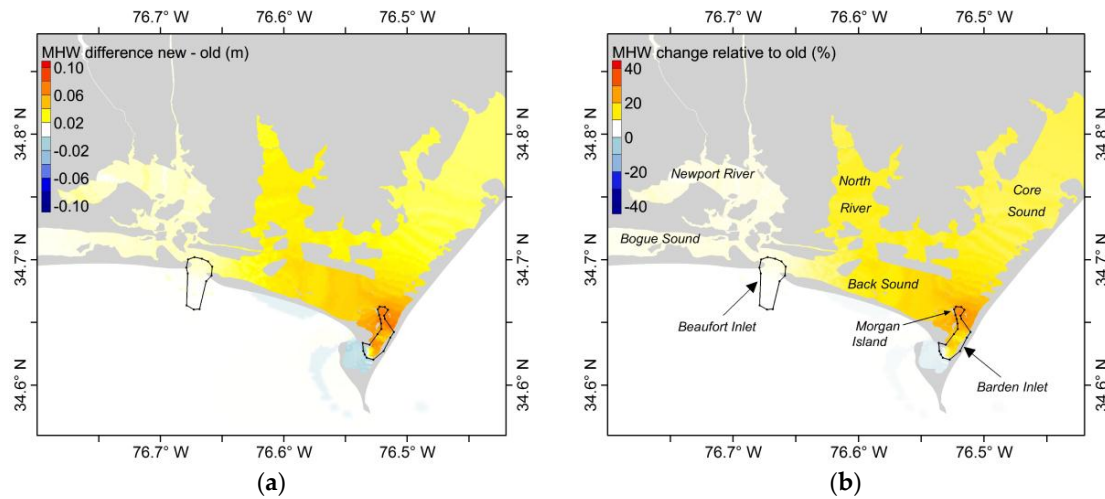


Figure 11. The MHW changes induced only by the inlet morphological changes around Barden Inlet: (a) the MHW difference between the new-bathy-BA model and the old-bathy model; (b) the MHW change in percentage relative to the old-bathy model MHW. The black dotted polygons delineate the area with changed bathymetry.

As shown in Figure 11, if the morphological changes only occurred around Barden Inlet (i.e., the new-bathy-BA model), the increased MHW has a maximum of 0.06 m (22% of the old MHW) around Morgan Island. The percentage of the increased MHW relative to the old MHW drops to 10% 7 km away from Morgan Island in the Back Sound direction and 3 km in the Core Sound direction. Thus, the inlet morphological changes have more influence on MHW in the Back Sound direction than in the Core Sound direction. This is probably because tidal changes induced by the inlet morphological changes are positively correlated with tidal range. Tidal range is larger due to less damped tidal energy in the deeper Back Sound relative to Core Sound (see depths in Figure 3a,b and MHW in Figure 12a,b).

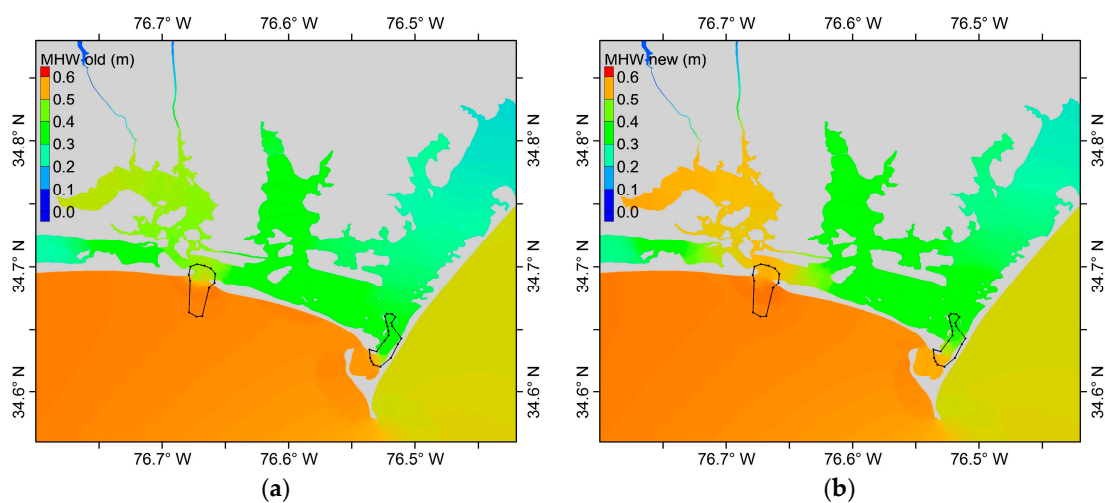


Figure 12. Cont.

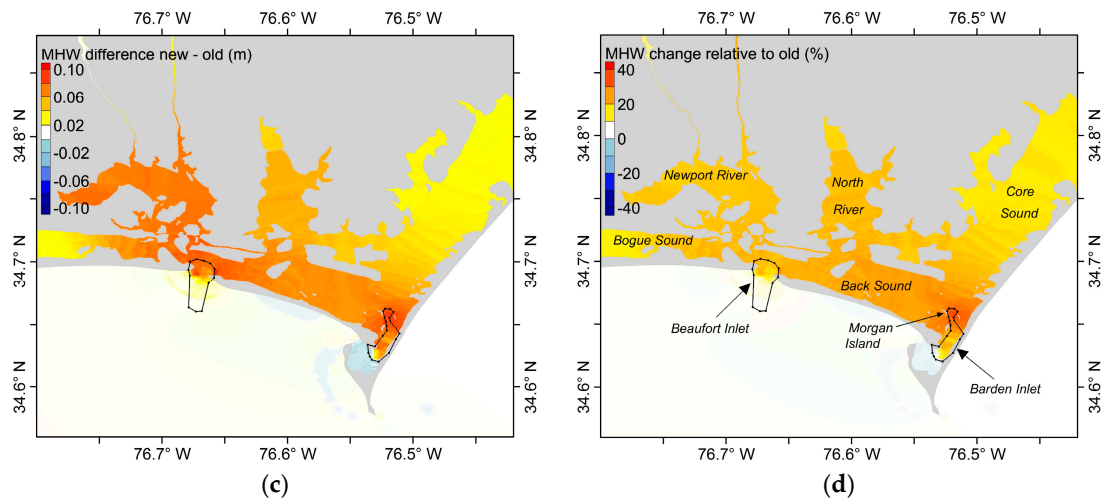


Figure 12. The MHW changes induced by the inlet morphological changes around Beaufort Inlet and Barden Inlet: (a) MHW from the old-bathy model; (b) MHW from the new-bathy model; (c) the MHW difference between the new-bathy model and the old-bathy model; (d) the MHW change in percentage relative to the old-bathy model MHW. The black dotted polygons delineate the area with changed bathymetry.

In fact, the morphological changes occurred around both Beaufort Inlet and Barden Inlet. As shown in Figure 12c, the increased MHW is almost the sum of that induced by individual inlet morphological changes. For example, the increased MHW in North River is about 0.04 m. About 0.02 m is from the morphological changes of Beaufort Inlet (Figure 10a). The other 0.02 m is from the morphological changes of Barden Inlet (Figure 11a). This is probably because the tides propagating through Beaufort Inlet interact with the tides propagating through Barden Inlet in the regions located in between both inlets. In the Core Sound direction, the location of the contour of 10% increase in MHW is 10 km (Figure 12d) away from Morgan Island, compared to 3 km in the new-bathy-BA model (Figure 11b). The extended part should come from the contribution of the Beaufort Inlet changes.

The influence range of the morphological changes around Ocracoke Inlet, Hatteras Inlet, and Oregon Inlet are shorter than the distances between itself and its neighbor inlets. Thus, the morphological changes of these three inlets have independent effects on local tidal datum changes.

For Ocracoke Inlet, water depths (Figure 4) have increased from ~4 m to ~9 m in the northeastern part of the ocean-side area of the inlet but have decreased from ~4 m to ~2 m in most sound-side areas of the inlet. As a result, MHW (Figure 13) has increased of ~20% from ~0.35 m to ~0.42 m in the middle of the inlet and the increased MHW is confined within the inlet. MHW has a sudden drop by ~20% from ~0.21 m to ~0.17 m on the northeastern side behind the inlet and the decreased MHW extends inside of Pamlico Sound. The percentage of the decreased MHW gradually drops to 10% about 6 km behind the inlet in the northeastern direction. Therefore the decreased water depths at the inside entrance play a key role in strengthening the tides within the inlet but weakening the tides behind the inlet.

For Hatteras Inlet, water depths (Figure 4) have decreased from ~5 m to ~2 m on the eastern side of the inlet, which leads to a MHW (Figure 13) drop of ~30% from ~0.25 m to ~0.17 m. The decreased MHW also extends inside of Pamlico Sound. The percentage of the decreased MHW gradually drops to 10% about 4 km behind the inlet in the northeastern direction. Water depths have increased from ~1 m to ~4 m on the western side of the inlet, which leads to a MHW increase of ~20% from ~0.23 to ~0.28. The extension of the increased MHW is confined within a small area inside the inlet and may be due to the decreased water depths in the western part of the inside entrance.

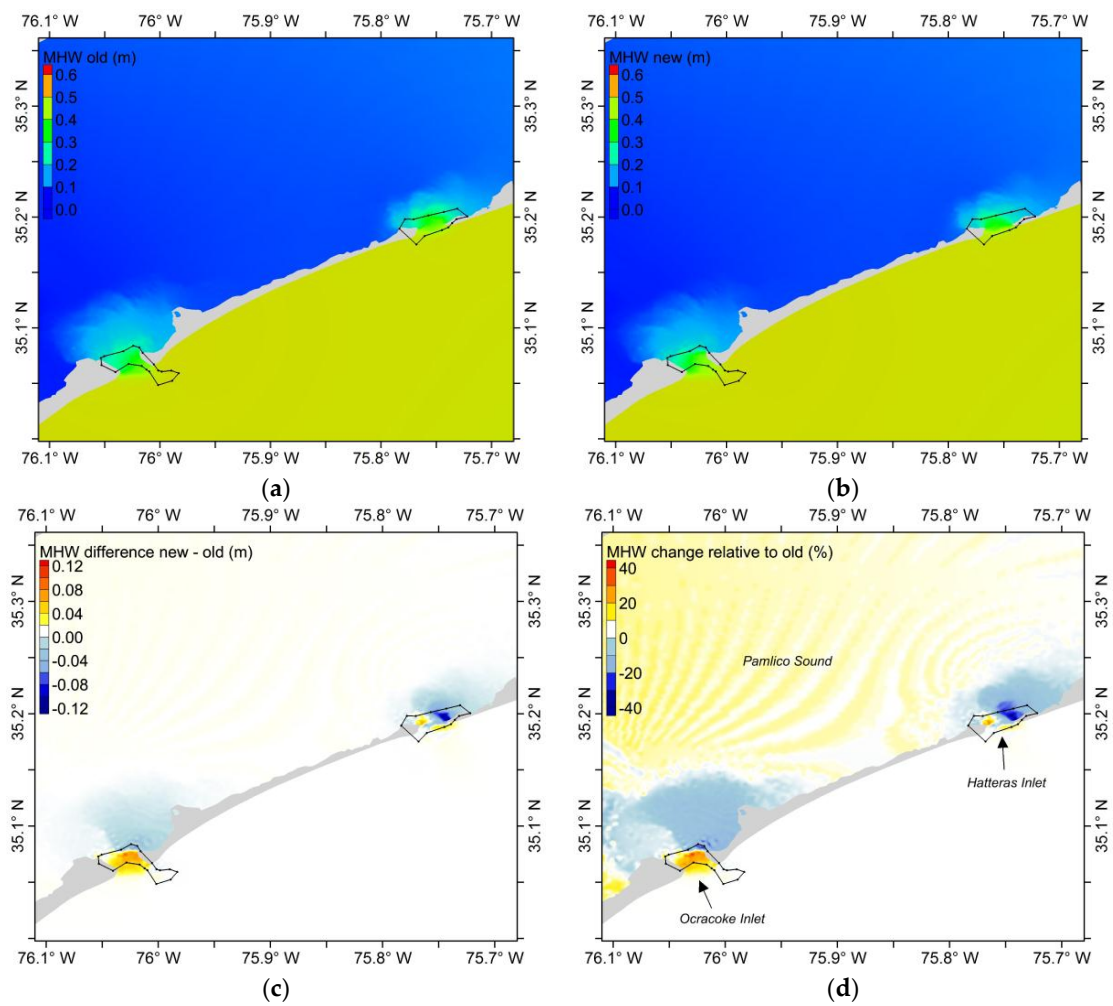


Figure 13. The MHW changes induced by the inlet morphological changes around Ocracoke Inlet and Hatteras Inlet: (a) MHW from the old-bathy model; (b) MHW from the new-bathy model; (c) the MHW difference between the new-bathy model and the old-bathy model; (d) the MHW change in percentage relative to the old-bathy model MHW. The black dotted polygons delineate the area with changed bathymetry.

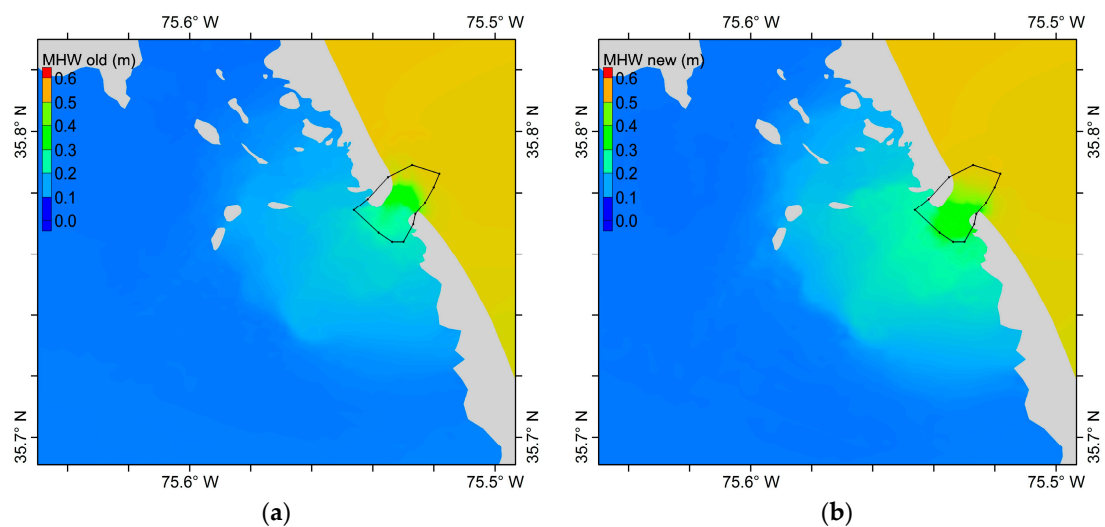


Figure 14. Cont.

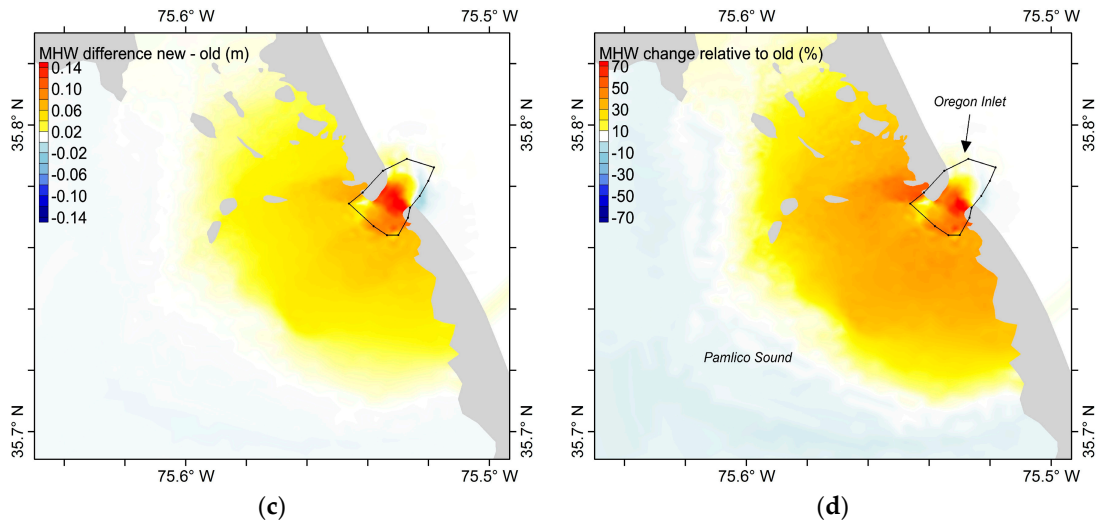


Figure 14. The MHW changes induced by the inlet morphological changes around Oregon Inlet: (a) MHW from the old-bathy model; (b) MHW from the new-bathy model; (c) the MHW difference between the new-bathy model and the old-bathy model; (d) the MHW change in percentage relative to the old-bathy model MHW. The black dotted polygons delineate the area with changed bathymetry.

For Oregon Inlet, the inlet channel with ~8 m depth has shifted from the northwestern side in the old-bathy grid to the southeastern side in the new-bathy grid (Figure 5). The average depth around Oregon Inlet has increased from ~3.6 m of the old-bathy grid to ~4.0 m of the new-bathy grid. Unlike Ocracoke Inlet and Hatteras Inlet, MHW (Figure 14) has increased by ~50% from ~0.25 m to ~0.37 m across the interior of the inlet. The increased MHW extends inside of Pamlico Sound. The percentage of the increased MHW gradually drops to 10% about 6 km behind the inlet in almost all directions. This is probably because the presence of several deeper channels (Figure 5a,b) in Pamlico Sound behind Oregon Inlet favors tidal propagation in all directions.

3.2. Tidal Harmonic Changes

The spatial pattern of the M_2 amplitude in North Carolina coastal waters is similar to that of MHW because M_2 is the dominant component of tidal constituents in this region; consequently, the M_2 amplitude changes induced by the inlet morphological changes are also similar to the MHW changes. Figure 15a,b show the M_2 amplitude and phase from the old-bathy model and the new-bathy model along a line (shown in Figure 2b) approximately 1 km behind the barrier islands. The M_2 amplitude has increased from the old-bathy model to the new-bathy model behind Beaufort Inlet, Barden Inlet, and Oregon Inlet and has decreased behind Ocracoke Inlet and Hatteras Inlet. The M_2 phase has slightly decreased from the old-bathy model to the new-bathy model behind Beaufort Inlet, Barden Inlet, and Oregon Inlet and has changed very little behind Ocracoke Inlet and Hatteras Inlet. These suggest that it becomes easier for the M_2 tide to propagate through Beaufort Inlet, Barden Inlet, and Oregon Inlet relative to about 40 or 60 years ago. It becomes more difficult for the M_2 tide to propagate through Ocracoke Inlet and Hatteras Inlet relative to about 50 or 80 years ago.

As shown in Figure 15c,d, the K_1 amplitude and phase changes induced by the inlet morphological changes are similar to the M_2 amplitude and phase changes. However, when we compared the percentage of the amplitude change relative to the old, we found that the K_1 changes are less dramatic than the M_2 changes behind Beaufort Inlet and Barden Inlet (Figure 16). The K_1 changes in percentage have similar magnitudes to the M_2 changes behind Ocracoke Inlet, Hatteras Inlet, and Oregon Inlet.

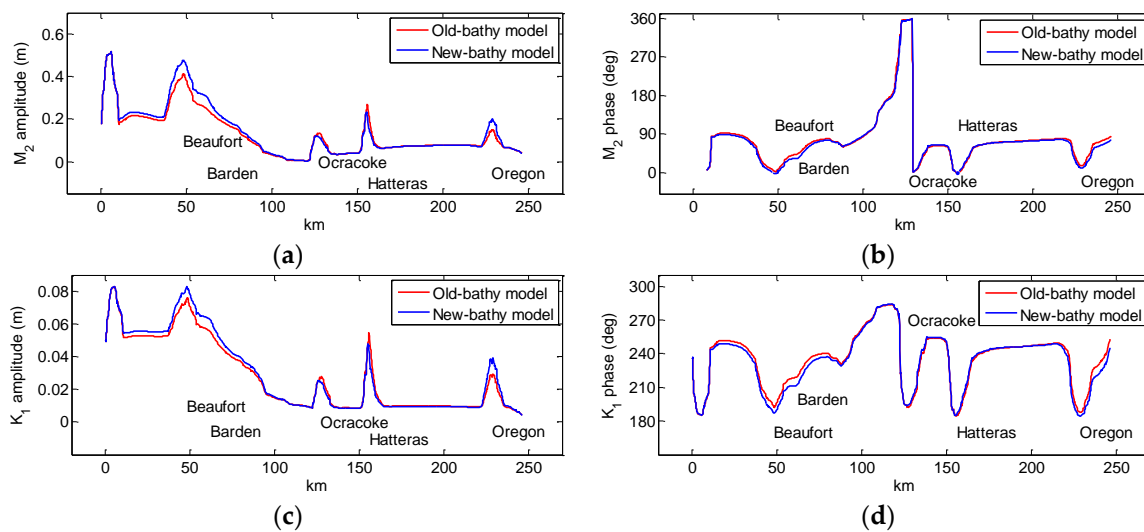


Figure 15. Longitudinal variations of: (a) the M_2 amplitude; (b) the M_2 phase; (c) the K_1 amplitude; (d) the K_1 phase along a line (shown in Figure 2b) about 1 km behind the barrier islands. The red lines indicate the results from the old-bathy model. The blue lines indicate the results from the new-bathy model.

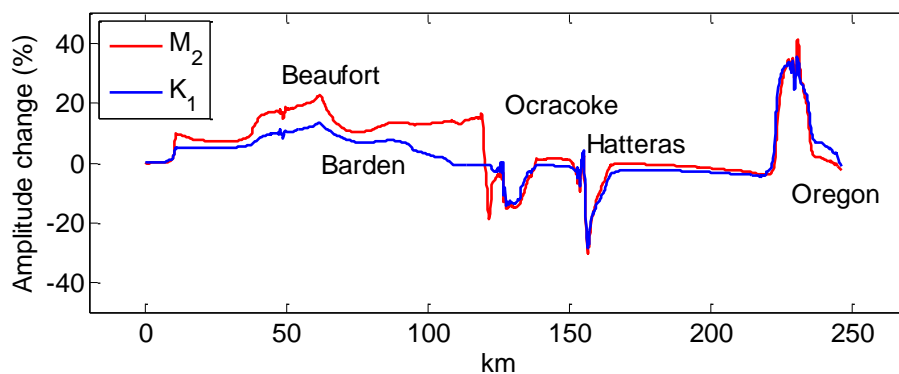


Figure 16. Comparison between the M_2 (red line) and K_1 (blue line) in amplitude change between the new-bathy model and the old-bathy model relative to the old-bathy model along a line (shown in Figure 2b) about 1 km behind the barrier islands.

4. Discussion and Conclusions

The model results validated with the observations show that tidal datums (represented by MHW) and harmonic amplitudes have increased by 10%–35% from the old-bathy model to the new-bathy model behind Beaufort Inlet, Barden Inlet, and Oregon Inlet. Tidal datums and harmonic amplitudes have decreased by 15%–30% from the old-bathy model to the new-bathy model behind Ocracoke Inlet and Hatteras Inlet. Compared with the other four inlets, tidal datums around Oregon Inlet experienced the most dramatic changes (35%) within a shorter time period (1975–2014). The reason needs to be further investigated. In addition, Beaufort Inlet has the largest range of influence probably due to the deeper waters behind it.

It should be noted that all four tidal datums (MHHW, MHW, MLW, and MLLW) are referenced to MSL. The MHHW, MLW, and MLLW changes induced by the inlet morphological changes are very similar to the MHW changes. Tidal range is an indicator of tidal energy. The morphological changes of the inlets affect the energy of the tides propagating through the inlets and thus tidal range behind the inlets. MHW and MLW are almost equal to half of the mean tidal range. MHHW and MLLW are

almost equal to half of the diurnal tidal range. Therefore, all four tidal datums have similar changes in response to the morphological changes.

To evaluate these tidal changes induced by morphological changes of the inlets, we calculated the flood and ebb volumes and durations across the inlets based on the velocity and elevation outputs from the old-bathy model and the new-bathy model. The results have been summarized in Table 3. For Beaufort Inlet, the flood volume has increased by $18 \times 10^6 \text{ m}^3$ (16%) while the ebb volume has increased by $8 \times 10^6 \text{ m}^3$ (7%) from the old-bathy model to the new-bathy model, suggesting that more tidal energy and more water go into the sounds. Similarly, flood volumes have increased by $8 \times 10^6 \text{ m}^3$ (38%) and $11 \times 10^6 \text{ m}^3$ (15%) for Barden Inlet and Oregon Inlet, respectively. On the other hand, flood volumes have decreased by $5 \times 10^6 \text{ m}^3$ (4%) and $7 \times 10^6 \text{ m}^3$ (6%) for Ocracoke Inlet and Hatteras Inlet, respectively. These suggest that the cross-inlet tidal volume changes are closely related to tidal datum changes behind the inlets. The magnitude of the volume change is also positively correlated with the influence range.

Table 3. Flood and ebb volumes and durations across five North Carolina inlets from the old-bathy model and the new-bathy model.

Inlet	Flood Volume (10^6 m^3)	Ebb Volume (10^6 m^3)	Tidal-Cycle Residual (10^6 m^3)	Flood Duration (h)	Ebb Duration (h)
Beaufort (old)	111.31	-113.60	-2.29	5.95	6.53
Beaufort (new)	129.37	-121.43	7.95	5.99	6.48
Barden (old)	21.72	-18.76	2.96	5.92	6.56
Barden (new)	30.02	-27.67	2.36	5.96	6.51
Ocracoke (old)	132.47	-141.34	-8.87	5.79	6.71
Ocracoke (new)	127.09	-132.91	-5.81	5.77	6.73
Hatteras (old)	122.12	-122.90	-0.78	5.80	6.70
Hatteras (new)	114.87	-113.74	1.13	5.80	6.70
Oregon (old)	73.07	-73.63	-0.56	5.82	6.67
Oregon (new)	84.52	-84.30	0.22	5.84	6.66

As mentioned in Section 2.2, for the common regions other than the inlet regions, the old-bathy grid and the new-bathy grid used the same bathymetry sounding datasets [27]. For the shallow areas within the sounds, most sounding data were collected before the 1980s and very limited sounding data were collected after the 2010s. Tidal changes induced by morphological changes within the sounds will be evaluated in future work upon the availability of new sounding data in these regions.

Based on the numerical experiments in this paper, both the magnitude and geographical extension of the tidal datum changes behind the barrier islands can be easily evaluated by monitoring the inlet morphological changes induced by erosion or accumulation, dredging, or dumping. This can be used as a guidance for NOAA to make decisions on when to update VDatum tidal datums in this region and where to install new tide gauges. Furthermore, as the sea level may rise in the future, some new inlets may appear and the existing inlets may become wider and deeper. Under this circumstance, the spatial pattern of the tides behind the barrier islands may be dramatically changed, which will be evaluated in future work.

Acknowledgments: This study was supported by NOAA’s VDatum program coordinated by three NOAA offices: the Office of Coast Survey, the Center for Operational Oceanographic Products and Services, and the National Geodetic Survey. We sincerely thank the anonymous reviewers for providing insightful comments and suggestions to help substantial improvements of this manuscript.

Author Contributions: J.W. and E.M. conceived and designed the experiments; J.W. performed the experiments and analyzed the data; J.W. and E.M. wrote the paper.

Conflicts of Interest: The authors declare no conflict of interest.

References

1. Parker, B.B.; Hess, K.W.; Milbert, D.G.; Gill, S. A national vertical datum transformation tool. *Sea Technol.* **2003**, *44*, 10–15.
2. Eakins, B.W.; Taylor, L.A. Seamlessly integrating bathymetric and topographic data to support tsunami modeling and forecasting efforts. In *Ocean Globe*; Bremen, J., Ed.; ESRI Press Academic: Redlands, CA, USA, 2010; pp. 33–86.
3. National Ocean Service. *Tidal Datums and Their Applications*; NOAA Technical Report NOS COOPS 1; Center for Operational Oceanographic Products and Services: Silver Spring, MD, USA, 2000; p. 112.
4. National Ocean Service. *VDatum Manual for Development and Support of NOAA's Vertical Datum Transformation Tool, VDatum*. 2012; p. 119. Available online: <http://vdatum.noaa.gov/docs/publication.html> (accessed on 20 September 2016).
5. Luettich, R.A., Jr.; Westerink, J.J.; Scheffner, N.W. *ADCIRC: An Advanced Three-Dimensional Circulation Model for Shelves Coasts and Estuaries, Report 1: Theory and Methodology of ADCIRC-2DDI and ADCIRC-3DL*; Dredging Research Program Technical Report DRP-92-6; U.S. Army Engineers Waterways Experiment Station: Vicksburg, MS, USA, 1992; p. 137.
6. Westerink, J.J.; Luettich, R.A.; Muccino, J.C. Modeling tides in the Western North Atlantic using unstructured graded grids. *Tellus A* **1994**, *46*, 178–199. [[CrossRef](#)]
7. Mukai, A.Y.; Westerink, J.J.; Luettich, R.A.; Mark, D. *Eastcoast 2001: A Tidal Constituent Database for the Western North Atlantic, Gulf of Mexico and Caribbean Sea*; Technical Report, ERDC/CHL TR-02-24; US Army Engineer Research and Development Center, Coastal and Hydraulics Laboratory: Vicksburg, MS, USA, 2002; p. 201.
8. Hench, J.L.; Luettich, R.A.; Westerink, J.J.; Scheffner, N.W. *ADCIRC: An Advanced Three-Dimensional Circulation Model for Shelves, Coasts, and Estuaries, Report 6: Development of a Tidal Constituent Database for the Eastern North Pacific*; Dredging Research Program Technical Report DRP-92-6; U.S. Army Engineer Waterways Experiment Station: Vicksburg, MS, USA, 1994; p. 21. Available online: <http://acwc.sdp.sirsi.net/client/search/asset/1004166> (accessed on 20 September 2016).
9. Blain, C.A.; Rogers, E. *Coastal Tidal Prediction Using the ADCIRC-2DDI Hydrodynamic Finite Element Model*; Formal Report NRL/FR/7322-98-9682; Naval Research Laboratory, Stennis Space Center: Hancock County, MS, USA, 1998; p. 92. Available online: <http://www.dtic.mil/dtic/tr/fulltext/u2/a358752.pdf> (accessed on 20 June 2016).
10. Luettich, R.A., Jr.; Carr, S.D.; Reynolds-Fleming, J.V.; Fulcher, C.W.; McNinch, J.E. Semi-diurnal seiche in a shallow, micro-tidal lagoonal estuary. *Cont. Shelf Res.* **2001**, *22*, 1669–1681. [[CrossRef](#)]
11. Burrows, R.; Walkington, I.A.; Yates, N.C.; Hedges, T.S.; Wolf, J.; Holt, J. The tidal range energy potential of the west coast of the United Kingdom. *Appl. Ocean Res.* **2009**, *31*, 229–238. [[CrossRef](#)]
12. Hess, K.; Spargo, E.; Wong, A.; White, S.; Gill, S. *VDatum for Central Coastal North Carolina: Tidal Datums, Marine Grids, and Sea Surface Topography*; NOAA Technical Report NOS CS 21; the National Oceanic and Atmospheric Administration: Silver Spring, MD, USA, 2005; p. 46.
13. Hayes, M.O. General morphology and sediment patterns in tidal inlets. *Sediment. Geol.* **1980**, *26*, 139–156. [[CrossRef](#)]
14. Hubbard, D.K.; Oertel, G.; Nummedal, D. The role of waves and tidal currents in the development of tidal-inlet sedimentary structures and sand body geometry: Examples from North Carolina, South Carolina, and Georgia. *J. Sediment. Petrol.* **1979**, *49*, 1073–1092.
15. Komar, P.D. Tidal-inlet processes and morphology related to the transport of sediments. *J. Coast. Res.* **1996**, 23–45.
16. Cayocca, F. Long-term morphological modeling of a tidal inlet: The Arcachon Basin, France. *Coast. Eng.* **2001**, *42*, 115–142. [[CrossRef](#)]
17. Militello, A.; Zarillo, G.A. Tidal motion in a complex inlet and bay system, Ponce de Leon Inlet, Florida. *J. Coast. Res.* **2000**, *16*, 840–852.
18. Boon, J.D.; Byrne, R.J. On basin hyposmetry and the morphodynamic response of coastal inlet systems. *Mar. Geol.* **1981**, *40*, 27–48. [[CrossRef](#)]
19. Fitzgerald, D.M. Geomorphic variability and morphologic and sedimentologic controls of tidal inlets. *J. Coast. Res.* **1996**, 47–71.

20. Luettich, R.A., Jr.; Hench, J.L.; Fulcher, C.W.; Werner, F.E.; Blanton, B.O.; Churchill, J.H. Barotropic tidal and wind driven larvae transport in the vicinity of a barrier island inlet. *Fish. Oceanogr.* **1999**, *8*, 190–209. [[CrossRef](#)]
21. Churchill, J.H.; Blanton, J.O.; Hench, J.L.; Luettich, R.A., Jr.; Werner, F.E. Flood tide circulation near Beaufort Inlet, North Carolina: Implications for larval recruitment. *Estuaries* **1999**, *22*, 1057–1070. [[CrossRef](#)]
22. Inman, D.L.; Dolan, R. The Outer Banks of North Carolina: Budget of sediment and inlet dynamics along a migrating barrier system. *J. Coast. Res.* **1989**, *5*, 193–237.
23. NOAA Tides and Currents Website: Water Levels. Available online: <http://tidesandcurrents.noaa.gov/stations.html?type=Water+Levels> (accessed on 20 September 2016).
24. NOAA Tides and Currents Website: Datums. Available online: <http://tidesandcurrents.noaa.gov/stations.html?type=Datums> (accessed on 20 September 2016).
25. NOAA Tides and Currents Website: Harmonic Constituents. Available online: <https://tidesandcurrents.noaa.gov/stations.html?type=Harmonic+Constituents> (accessed on 20 September 2016).
26. NOAA Shoreline Website. Available online: <https://shoreline.noaa.gov> (accessed on 20 September 2016).
27. National Centers for Environmental Information (NCEI) Bathymetry and Global Relief. Available online: <https://www.ngdc.noaa.gov/mgg/bathymetry/relief.html> (accessed on 20 September 2016).
28. Becker, J.J.; Sandwell, D.T.; Smith, W.H.F.; Braud, J.; Binder, B.; Depner, J.; Fabre, D.; Factor, J.; Ingalls, S.; Kim, S.-H.; et al. Global bathymetry and elevation data at 30 arc seconds resolution: SRTM30_PLUS. *Mar. Geod.* **2009**, *32*, 355–371. [[CrossRef](#)]
29. US Army Corps of Engineering Wilmington District Website: Hydrographic Surveys. Available online: <http://www.saw.usace.army.mil/Missions/Navigation/Hydrographic-Surveys/> (accessed on 20 September 2016).
30. Olsen Associates, Inc. Inlet Dredging and Disposal. In *Regional Sand Transport Study: Morehead City Harbor Federal Navigation Project Summary Report*; Olsen Associates, Inc.: Jacksonville, FL, USA, 2006. Available online: <http://www.carteretcountync.gov/DocumentCenter/View/268> (accessed on 20 June 2016).
31. NOAA VDatum Website: Estimation of Uncertainties. Available online: http://vdatum.noaa.gov/docs/est_uncertainties.html (accessed on 20 September 2016).



© 2016 by the authors; licensee MDPI, Basel, Switzerland. This article is an open access article distributed under the terms and conditions of the Creative Commons Attribution (CC-BY) license (<http://creativecommons.org/licenses/by/4.0/>).